1st Latin-American Workshop on Structural Health Monitoring
LATAM-SHM 2023
December, 5-8 2023

ADVANCING WIND TURBINE RELIABILITY: MACHINE LEARNING-BASED EARLY DETECTION OF ROTOR IMBALANCE FOR PROACTIVE MAINTENANCE STRATEGIES

Iván González[*], Ricardo Prieto-Galarza[†,‡], Christian Tutivén[*,‡] and Yolanda Vidal[‡,△]

[*] Mechatronics Engineering
Faculty of Mechanical Engineering and Production Science, FIMCP
Escuela Superior Politécnica del Litoral, ESPOL
Campus Gustavo Galindo Km. 30.5 Vía Perimetral, P.O. Box 09-01-5863, Guayaquil, Ecuador
Phone number: +593 9 9103 5259,
e-mail: {ivargonz, cjtutive}@espol.edu.ec,
Web page: https://www.espol.edu.ec

[†]Universidad Ecotec
Km. 13.5 Samborondón, Samborondón, EC092302 Ecuador.

[‡]Control, Data, and Artificial Intelligence, CoDAlab
Department of Mathematics, Escola d'Enginyeria de Barcelona Est, EEBE
Universitat Politècnica de Catalunya, UPC
Campus Diagonal-Besós (CDB) 08019, Barcelona, Spain
e-mail: {ricardo.prieto yolanda.vidal}@upc.edu,
Web page: https://www.upc.edu/

[△]Institut de Matemàtiques de la UPC
BarcelonaTech, IMTech
Pau Gargallo 14, 08028 Barcelona, Spain

Key words: wind turbine, rotor imbalance, vibration-data, predictive maintenance, machine learning, extended isolation forest

Abstract. This work presents a comprehensive methodology for early detection of rotor imbalance is crucial for maintaining the reliability and operational efficiency of wind turbines. It uses accelerometer data, focusing solely on vibration responses, and employs advanced machine learning, particularly the extended isolation forest. The process involves collecting and processing accelerometer data to extract relevant features that capture the characteristic patterns of the vibration signals associated with rotor imbalance. An extended isolation forest model is trained exclusively on data from healthy wind turbines, enabling precise anomaly detection and proactive maintenance. Experimental validation on a controlled rotor imbalance in a laboratory-scale wind turbine demonstrating the feasibility and effectiveness of the proposed methodology. Results emphasize its capability to detect and diagnose rotor imbalance faults, providing an early warning system for turbine operators. This approach addresses the main objective of detecting rotor imbalance and contributes to the advancement of predictive maintenance strategies in the wind energy industry.

1 INTRODUCTION

In today's world, the global pursuit of sustainable and renewable energy sources has fueled significant advancements in wind energy technologies. Wind turbines (WTs), by harnessing the kinetic power of the wind to produce electricity, play a pivotal role in green energy generation. The continued viability of wind energy hinges on ensuring the reliability and operational efficiency of these complex machines, where the correct operation of WTs is paramount in the context of renewable energy generation. However, WTs encounter various environmental and mechanical challenges throughout their operational lifespans, and among these challenges, rotor imbalance emerges as a critical, can result in efficiency losses and decreased lifetime of bearings and other components, leading to system fault and significant safety risk [1, 2]. As the global reliance on wind energy continues to grow, so does the importance of addressing the issue of rotor imbalance. Nevertheless, rotor imbalance is omnipresent in all rotating machinery, posing serious threat to machine life and operation [3] which poses a substantial threat to the performance and longevity of WT systems. Hence, the early detection of rotor imbalance takes on even greater significance, as it is the linchpin for ensuring the continued reliability and operational efficiency of WTs in the pursuit of sustainable energy sources. Left unaddressed, rotor imbalance can lead to severe consequences, including increased wear on critical components, reduced energy generation efficiency, and structural damage to the WT [4].

In the realm of rotor imbalance detection, diverse methodologies have been investigated to enhance the identification and resolution of this issue. A notable contribution is the work of Cacciola et al. [5], which introduced an innovative approach utilizing harmonic analysis of rotor responses in the fixed frame to discriminate between various imbalance sources. Furthermore, recent research by Wisal and Oh [1] has introduced a novel approach that integrates ResNet and CNN techniques, resulting in significantly improved accuracy in classifying rotor imbalances. These advancements contribute to the field of rotor imbalance detection by providing more effective and accurate methods for addressing this critical concern.

This work addresses the critical challenge of rotor imbalance detection in WTs by introducing an innovative approach that combines accelerometer data for vibration responses with advanced machine learning techniques, specifically the Extended Isolation Forest (EIF) algorithm, known for its efficacy in anomaly detection. The methodology is rigorously validated through experiments on a laboratory-scale WT with controlled rotor imbalance, showing its great effectiveness in detecting rotor faults. Furthermore, considering the time series nature of the data, it was possible to clearly distinguish between healthy situations and faults. These results support the capability of early anomaly detection, results that not only have critical implications in terms of maintenance efficiency, but also reduce repair costs and ensure the long-term operation of wind turbines. Timely identification of imbalance issues allows for proactive maintenance strategies, minimizing downtime, reducing repair costs, and ensuring the long-term functionality of WTs.

The document is organized in the following manner. Section 2 describes the experimental setup, of the laboratory-scale WT. Section 3 details the methods used to build the EIF-based damage detection model. Section 4, describes the obtained results. Lastly, Section 5 provides the main conclusions and outlines directions for future research.

2 EXPERIMENTAL SETUP

In this Section, the experimental setup is described. First, a small WT is used, namely the E30Pro WT, which is specifically adapted for laboratory needs; see Figure 1. The turbine is conditioned to be powered by electric current, which makes it possible to control its start-up, facilitating the collection of data.

Figure 1: E30Pro scaled-down version of a WT.

The main focus of the methodology employed in this work is to exclusively use vibration measurements. To carry out these measurements, eight triaxial accelerometers (PCB® Piezotronic model 356A17) are installed in the turbine structure, as illustrated in Figure 2. These accelerometers are connected to six National Instruments™ cartridges (NI 9234 model), that are inserted in the National Instruments chassis cDAQ-9188. Finally, the Data Acquisition Toolbox™ is used to configure the data acquisition hardware and to log and analyze the data into the MATLAB® environment.

This work addresses the problem of detecting a fault due to an imbalance of the rotor of a WT by adding a mass of 575 g on one of the blades. This scenario represents realistic rotor imbalance situations that can occur during the operation of a WT. On the other hand, there is also the reference state, or healthy state, which is obtained when none of the blades has an additional mass.

3 METHODOLOGY

In this section of the methodology, an overview of the key steps followed in the research is presented. It begins by detailing the data acquisition process, followed by the reorganization of the data for further analysis. Then, it is explained how relevant features are extracted from these data. Next, the construction of a characteristic matrix essential for analysis is described.

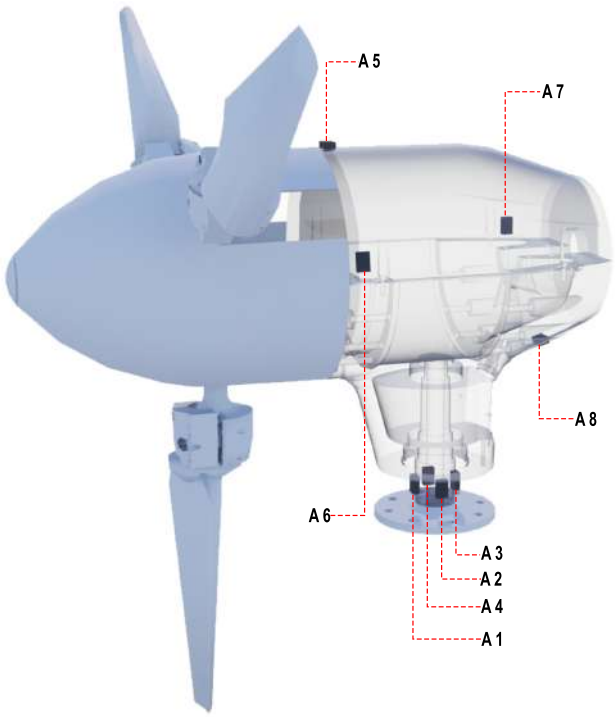

Figure 2: Location of the accelerometers on the WT.

It goes on to explain how the data are divided into training, validation and test sets, and how the values are normalized. Finally, the use of the EIF algorithm for accurate anomaly detection in the WT data is highlighted. These methodological steps provide a solid foundation for research, enabling rigorous analysis of the health and performance of the WT, which is critical in the context of wind asset engineering and management.

3.1 Hypothesis

This section shows the hypothesis on which the proposed rotor fault detection methodology is based. The online methodology involves acquiring an initial set of healthy data that is used to train the model and define a fault detection threshold. A second set of data is then collected, just to validate the model and ensure that it generalizes and that its hyperparameters are well selected. For a new diagnosis of the turbine rotor, several groups of data (test set) of 60 seconds each are collected. Finally, based on the test set of experiments, the diagnosis of the state is made.

3.2 Data Acquisition

A total of 55 experiments are performed, of which 50 are with the completely healthy WT and the rest simulating the added mass. A detailed description of the experiments performed is presented below:

- Fifty experiments in healthy conditions of the structure, that is, without alterations of the WT blades.
- Five experiments with 575 g weight increase in only one blade.

The duration of each experimental trial for data acquisition is 60 seconds, with a sampling rate of approximately 1706, 66 kHz. As a result, each of the 24 sensors records 102400 data measurements. Finally, the data associated to the k-th experiment is stored in matrix $\mathbf{X}^{(k)}$ with coefficients $x_{n,m}^{(k)}$ ($n = 1, \ldots, N$, $m = 1, \ldots, M$) that reads as

$$X^{(k)} = \begin{bmatrix} x_{1,1}^{(k)} & x_{1,2}^{(k)} & \ldots & x_{1,M}^{(k)} \\ x_{2,1}^{(k)} & x_{2,2}^{(k)} & \ldots & x_{2,M}^{(k)} \\ \vdots & \vdots & \ddots & \vdots \\ x_{N,1}^{(k)} & x_{N,2}^{(k)} & \ldots & x_{N,M}^{(k)} \end{bmatrix}, \tag{1}$$

considering $k \in [1, K]$, where K is 55. The two subindices, in the matrix coefficients, are related to the time instant (row) and sensor (column), respectively. More precisely,

- $n = 1, \ldots, N$ identifies the time stamp, while N is the number of time stamps per experiment, equal to 102400;
- $m = 1, \ldots, M$ represents the measuring sensor, while M is the total number of sensors, equal to 24.

As a result, each experiment matrix $X_{N,M}^{(k)} \in \mathbb{M}_{102400\times 24}^{(k)}(\mathbb{R})$.

3.3 Data Split

The $X^{(k)}$ matrix, which houses the acquisition data, as shown in Eq. 1, consists of a total of 55 experiments, is subjected to a splitting strategy into three distinct groups. The assignment of data to each group is performed as follows:

- Thirty-seven healthy experiments, equivalent to 75% of the healthy dataset are allocated to train the EIF model. This training dataset enables the EIF model to learn and capture patterns specific to normal WT operating conditions.
- Five healthy experiments equivalent to 10% of the healthy dataset are reserved for validating the EIF model. This portion of data is used to fit the EIF model hyperparameters and ensure proper generalization to unseen data.
- Eight healthy experiments equivalent to 15% of the healthy dataset and the entire fault dataset (comprising 5 experiments) are employed in the testing phase of the algorithm. This combined dataset is utilized to assess the algorithm's effectiveness in detecting fault conditions while also verifying its robustness in identifying data under normal operating conditions.

It is critical to emphasize that both training and validation are performed exclusively on healthy data, allowing the EIF model to robustly learn normal operating characteristics.

3.4 Data Reshape

In this section, data reshaping is being carried out to properly obtain multiple measurements from each sensor, providing greater insight into the state of the WT. The procedure is as follows:

1. Each column of the original matrix from Eq. (1) is divided into 32 sequences, where each one forms a row vector composed of 3200 consecutive measurements.
2. This is repeated for all columns, generating submatrices for each sensor.
3. Finally, the submatrices are concatenated one next to the other (maintaining the same order of the sensors).

Therefore, a new matrix $Z^{(k)}$ is obtained as shown in Eq. (2).

$$Z^{(k)} = \left[\; Z^{(k),1} \;\middle|\; Z^{(k),2} \;\middle|\; Z^{(k),3} \;\middle|\; Z^{(k),4} \;\middle|\; \cdots \;\middle|\; Z^{(k),M} \; \right], \tag{2}$$

where each submatrix $Z^{(k),m}$ is represented by

$$Z^{(k),m} = \begin{bmatrix} x^{(k)}_{1,m} & \cdots & x^{(k)}_{O,m} \\ x^{(k)}_{O+1,m} & \cdots & x^{(k)}_{2\cdot O,m} \\ \vdots & \ddots & \vdots \\ x^{(k)}_{(J-1)\cdot O+1,m} & \cdots & x^{(k)}_{J\cdot O,m} \end{bmatrix} = \begin{bmatrix} z^{(k),m}_{1,1} & \cdots & z^{(k),m}_{1,O} \\ z^{(k),m}_{2,1} & \cdots & z^{(k),m}_{2,O} \\ \vdots & \ddots & \vdots \\ z^{(k),m}_{J,1} & \cdots & z^{(k),m}_{J,O} \end{bmatrix}, \tag{3}$$

where O represents the length of a sequence, which is determined by considering the time intervals during which the blade can complete a 180-degree turn while minimizing the inclusion of unused observations, and $j = 1, \ldots, J$ identifies the sequence number, while J is the number of sequences per experiment, equal to 32. As a result, each matrix $Z^{(k),m} \in \mathbb{M}_{32\times 3200}(\mathbb{R})$.

This data-reshaping process enhances the richness of available information and significantly contributes to the next steps of the proposed methodology.

3.5 Feature Extraction

In the pursuit of gaining deeper insights into the behavior of the gathered WT data, the process of feature extraction emerges as a pivotal stage in data processing and signal analysis. These features serve as quantitative metrics, delivering pertinent insights into the nature of the recorded signals. The detailed descriptions of the three functions utilized within this framework are delved below. Each of these functions is meticulously applied to each of the matrices from Eq. (3).

3.5.1 Permutation Entropy

Permutation Entropy (PE) serves as a robust metric in time series analysis, offering insights into the probability distributions of potential system states and, consequently, the inherent information within them [6]. The concept of PE is built upon the Eq. (4):

$$\mathrm{PE}(z^{(k),m}_{j,\cdot}) = -\sum_{l=1}^{n!} p(\pi_l)\log(p(\pi_l)), \tag{4}$$

where:

- $\mathrm{PE}(z_{j,\cdot}^{(k),m})$ represents the PE of the j^{th} row of $Z^{(k),m}$ matrix.
- $n!$ is the factorial of n, indicating the total number of possible ordinal patterns or permutations of length n.
- $p(\pi_l)$ is the relative frequency of the l^{th} permutation π_l in the time series.

This Eq.(4), as introduced by Bandt and Pompe [7], forms the foundation of this analysis. The selection of the dimension n and the delay τ is pivotal for accurate computation. Guided by the comprehensive study by Audun Myers, et al. [8], which delves deep into the optimal parameter choices, this analysis adopts $n = 6$ and $\tau = 1$ as part of the feature extraction methodology. Here, $n = 6$ signifies the consideration of all feasible permutations of six consecutive values within each data segment. Concurrently, the $\tau = 1$ delay ensures a meticulous assessment of the relationships between successive data points in the series.

3.5.2 Fractal Dimension

Fractal dimension (FD) algorithms serve as powerful tools to analyze chaotic behavior in irregular time series, often represented as waveforms. These algorithms extract information about their geometrical structure at multiple scales.[9]. In this context, the FD is computed using the formula proposed by M. Katz [10], as shown in Eq. (5).

$$\mathrm{FD}(z_{j,\cdot}^{(k),m}) = \frac{\log(O)}{\log\left(\frac{d(z_{j,\cdot}^{(k),m})}{L(z_{j,\cdot}^{(k),m})} + 1\right)}, \tag{5}$$

where

- $\mathrm{FD}(z_{j,\cdot}^{(k),m})$ denotes the Katz's fractal dimension for the j^{th} row of $Z^{(k),m}$ matrix.
- $L(z_{j,\cdot}^{(k),m})$ represents the length of the curve for the j^{th} row, calculated as the cumulative sum of the Euclidean distances between successive points in the signal.
- $d(z_{j,\cdot}^{(k),m})$ is the maximum distance from any point in the signal to the initial point, essentially indicating the largest difference between the signal values in the j^{th} row of the $Z^{(k),m}$ matrix and the initial signal value.

The interplay between $L(z_{j,\cdot}^{(k),m})$ and $d(z_{j,\cdot}^{(k),m})$ offers invaluable insights into the fractal structure of the signal. Such understanding is pivotal for interpreting the nature of data acquired by specific sensors in the WT. Characterizing the signal in terms of its fractality is paramount to unveiling the underlying patterns and regularities. This, in turn, enhances the efficacy of WT performance analysis and monitoring.

3.5.3 Kurtosis

Kurtosis (Kurt), in the context of this study, is a statistical measure used to assess the shape of the data distribution, and is defined by the Eq. (6). This metric is applied individually to each row of the $Z^{(k),m}$ to quantify the "sharpness" or "flatness" of the corresponding signal. The following is the mathematical formula for computing kurtosis.

$$\text{Kurt}(z_{j,\cdot}^{(k),m}) = \frac{1}{O}\sum_{o=1}^{O}\left(\frac{z_{j,o}^{(k),m} - \bar{z}_{j,\cdot}^{(k),m}}{\sigma_{j,\cdot}^{(k),m}}\right)^4, \tag{6}$$

where

- $\text{Kurt}(z_{j,\cdot}^{(k),m})$ denotes the kurtosis for the j^{th} row of $Z^{(k),m}$ matrix.
- $\bar{z}_{j,\cdot}^{(k),m}$ is the mean of the row $z_{j,\cdot}^{(k),m}$
- $\sigma_{j,\cdot}^{(k),m}$ is the standard deviation of the row $z_{j,\cdot}^{(k),m}$

3.5.4 Construction of the Characteristic Matrix

In this section, we elucidate the construction of the final matrix, symbolized as $\widehat{Z}$, as depicted in (7). This matrix encapsulates the calculated metrics.

$$\widehat{Z}^{(k),m} = \begin{bmatrix} \text{PE}(z_{1,\cdot}^{(k),m}) & \text{FD}(z_{1,\cdot}^{(k),m}) & \text{Kurt}(z_{1,\cdot}^{(k),m}) \\ \text{PE}(z_{2,\cdot}^{(k),m}) & \text{FD}(z_{2,\cdot}^{(k),m}) & \text{Kurt}(z_{2,\cdot}^{(k),m}) \\ \vdots & \vdots & \vdots \\ \text{PE}(z_{J,\cdot}^{(k),m}) & \text{FD}(z_{J,\cdot}^{(k),m}) & \text{Kurt}(z_{J,\cdot}^{(k),m}) \end{bmatrix}, \tag{7}$$

where each row within $\widehat{Z}^{(k),m}$ contains the PE, FD, and Kurt metrics computed for the 3200 consecutive measurements of Eq. 3. Finally, a new matrix is obtained, as shown in the following Eq. 8:

$$\widehat{Z}^{(k)} = \left[\ \widehat{Z}^{(k),1} \ \middle|\ \widehat{Z}^{(k),2} \ \middle|\ \widehat{Z}^{(k),3} \ \middle|\ \widehat{Z}^{(k),4} \ \middle|\ \dots \ \middle|\ \widehat{Z}^{(k),M}\ \right]. \tag{8}$$

This matrix architecture offers a systematic approach to scrutinizing the temporal variations of these metrics and their association with individual sensors. The meticulous arrangement of PE, FD, and Kurt values within each sensor-specific submatrix augment the detection of patterns, trends, and potential anomalies in the WT's behavior. Serving as the analytical foundation, $\widehat{Z}^{(k)}$ is indispensable for a comprehensive understanding of the WT's operational performance and health. It further aids in pinpointing potential issues, be it in individual sensors or the turbine's holistic operation. Finally, each matrix $\widehat{Z}^{(k)} \in \mathbb{M}_{1760\times 72}(\mathbb{R})$.

3.6 Normalization

Normalization is performed using the Z-score method to standardize the characteristics, ensuring that they all contribute equally to the data analysis. This method, widely used in statistics and data analysis, is used to normalize variables, thus simplifying data comparison and processing. The Z-score is applied individually to each of the 72 columns of the $\widehat{Z}^{(k)}$ matrix in the training data set. Subsequently, the training mean and standard deviation values are used to normalize the validation and test sets (this is to avoid information leakage from training data to the other data sets). This ensured consistent normalization of all columns of the $\widehat{Z}^{(k)}$ matrix, preserving the relationship between the data in each column.

3.7 Extended Isolation Forest

Accurate anomaly detection is pivotal in this study, achieved through the application of the EIF algorithm, an extension of the Isolation Forest (iForest). EIF improves upon iForest by using hyperplanes with random slopes to separate the data, which effectively solves problems related to anomaly determination [11]. EIF constructs binary trees through random subsampling of the dataset, promoting a flexible approach to modeling anomalies. These trees divide the data based on randomly selected attributes, eventually reaching nodes with only one instance, which significantly enhances the isolation of anomalies. The anomaly score, reflecting the path length through the tree and ranging from 0 to 1, provides a clear indication of anomalies, with higher scores signifying their presence [12]. This extended approach introduces substantial improvements to anomaly detection, allowing for the identification of subtle anomalies in complex datasets, ultimately contributing to our study's comprehensive results and robust anomaly detection capabilities. The extension level can be adjusted based on the number of feature axes, which in this study ranges from 0 to 71, allowing for precise adaptation to the 72 available features. This range was chosen considering that a "fully extended" level would encompass all features but without redundancy, ensuring a tailored model fitting the data's feature count.

4 RESULTS

This section shows the obtained results. First, the hyperparameters for the EIF algorithm's architecture are determined using the training and validation datasets. To streamline this process, the Python framework Optuna is utilized for automated hyperparameter tuning. The hyperparameters outlined in Table 1 are obtained.

Table 1: Hyperparameters of the EIF algorithm.

Number of Trees	Size of subsample	Extension Level
369	1024	65

The results are presented using boxplots, where each $\widehat{Z}^{(k)}$ matrix corresponds to a one experiment. To evaluate the performance of the EIF algorithm, it is essential to use the training data as a reference. As can be seen in 3 (left) the maximum median of the anomaly score boxplots from all training experiments is equal to 0.48. This value is defined as the fault detection threshold for the validation and testing data set. Since the model is trained exclusively on data considered as "healthy", this threshold becomes a key reference. Any data falling below this threshold is classified as "healthy", while those above it are considered as "anomalous" or indicative of a fault. On the other hand, as can be seen in Figure 3 (right), none of the boxplots of the validation experiments exceed the predefined threshold, showing that the model generalizes well with the selected EIF hyperparameters.

To evaluate performance in healthy operating situations, test data corresponding to normal conditions are analyzed. In Figure 4, it can be seen that two healthy experiments are classified as anomalies. This does not mean that there exists a fault, since as indicated above, the detection is based on the analysis of the entire group of testing experiments.

On the other hand, Figure 5 depicts the analysis of test data related to rotor faults. In this

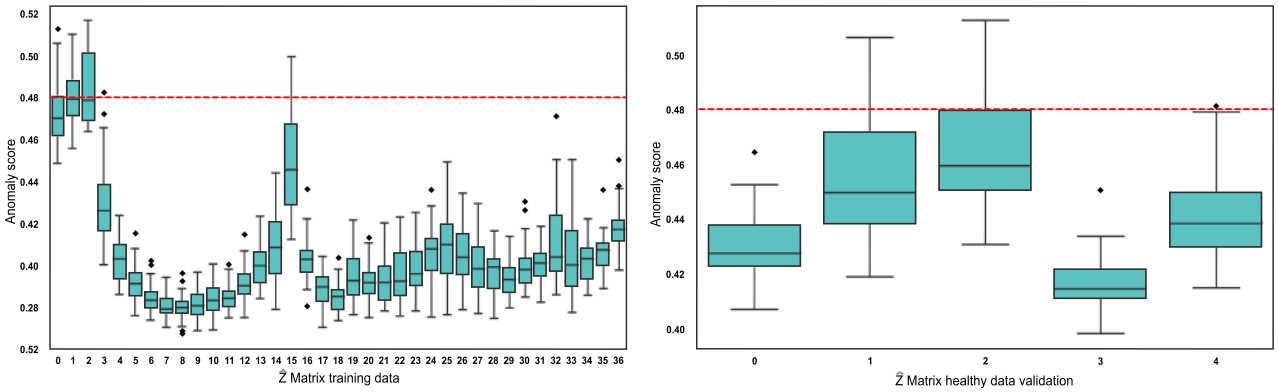

Figure 3: Boxplot of anomalies in training and validation data. The horizontal red dashed line represents the threshold value.

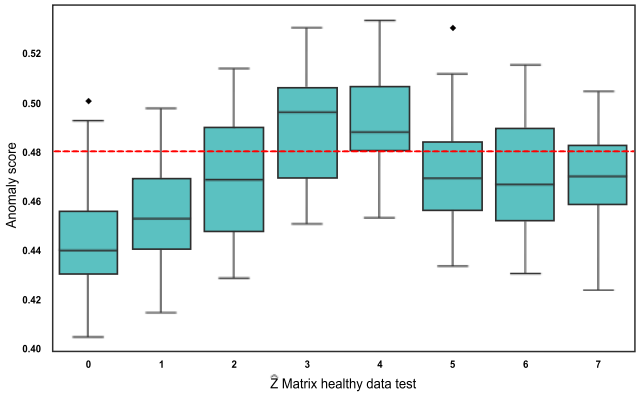

Figure 4: Boxplot of anomalies in health testing data. The horizontal red dashed line represents the threshold value.

case, it is observed that only one experiment falls below the established threshold. This does not mean that the rotor is healthy.

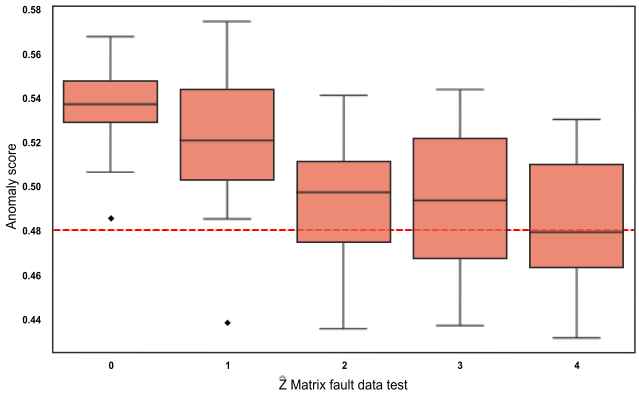

Figure 5: Boxplot of anomalies in fault testing data. The horizontal red dashed line represents the threshold value.

Since all of these data are time series, a grouping of all experiments considered "healthy" and

those with WT faults has been performed. This grouping has been performed to calculate an average anomaly score for each set, both for healthy running data and for data with faults. By considering the time-series nature, this approach allows us to gain a more robust perspective on the behavior of the WT throughout its normal operation and ultimately determine if it is faulty. These results are effectively represented in Figure 6. In this Figure, it is clearly seen that the mean of the anomaly scores for the "healthy" data is below the previously established threshold. On the other hand, the mean of the anomaly scores for the data classified as a "fault" is above the threshold. Furthermore, the separation between the two data sets is strikingly evident.

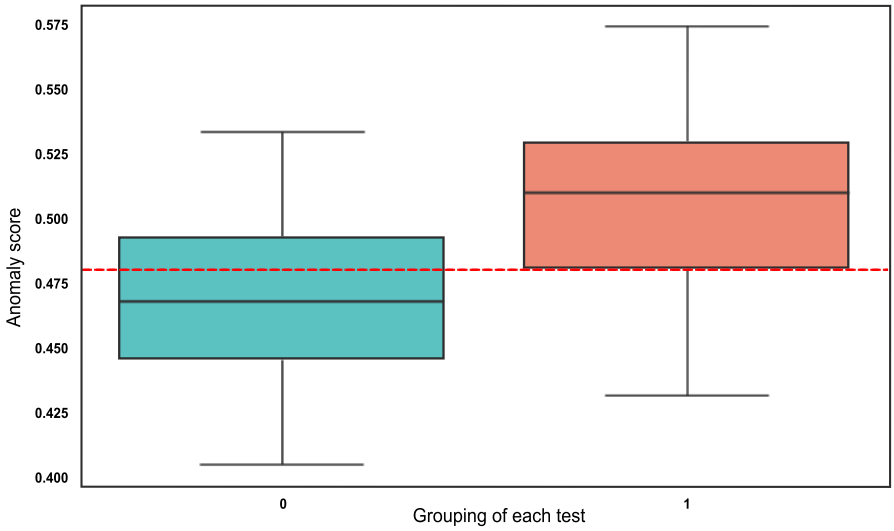

Figure 6: Classification of WT performance data. The horizontal red dashed line represents the threshold value.

These findings support an effective classification of the data, indicating that the EIF model is able to distinguish between normal operating situations and WT faults with a high degree of accuracy.

5 CONCLUSIONS

This paper has successfully addressed the critical challenge of early detection of rotor imbalance in WTs by implementing the EIF algorithm. The results obtained demonstrate the effectiveness of EIF in distinguishing between normal operating situations and faults in WTs with high accuracy. This approach has significant implications in terms of efficient maintenance and extended lifetime of wind turbines, thus contributing to the advancement of sustainable wind power generation. Future research could focus on optimizing this approach and its implementation in practical wind turbine monitoring applications on a larger scale.

REFERENCES

[1] M. Wisal, K.-Y. Oh, A new deep learning framework for imbalance detection of a rotating shaft, Sensors 23 (16) (2023) 7141.

[2] Á. Encalada-Dávila, B. Puruncajas, C. Tutivén, Y. Vidal, Wind turbine main bearing fault prognosis based solely on scada data, Sensors 21 (6) (2021) 2228.

[3] N. Ahobal, et al., Study of vibration characteristics of unbalanced overhanging rotor 577 (1) (2019) 012140.

[4] G. Hübner, H. Pinheiro, C. de Souza, C. Franchi, L. Da Rosa, J. Dias, Detection of mass imbalance in the rotor of wind turbines using support vector machine, Renewable Energy 170 (2021) 49–59.

[5] S. Cacciola, I. M. Agud, C. L. Bottasso, Detection of rotor imbalance, including root cause, severity and location, in: Journal of Physics: Conference Series, Vol. 753, IOP Publishing, 2016, p. 072003.

[6] M. Zanin, L. Zunino, O. A. Rosso, D. Papo, Permutation entropy and its main biomedical and econophysics applications: A review, Entropy 14 (8) (2012) 1553–1577.

[7] C. Bandt, B. Pompe, Permutation entropy: a natural complexity measure for time series, Physical review letters 88 (17) (2002) 174102.

[8] A. Myers, F. A. Khasawneh, On the automatic parameter selection for permutation entropy, Chaos: An Interdisciplinary Journal of Nonlinear Science 30 (3) (2020).

[9] F. Cervantes-De la Torre, J. I. González-Trejo, C. A. Real-Ramirez, L. F. Hoyos-Reyes, Fractal dimension algorithms and their application to time series associated with natural phenomena 475 (1) (2013) 012002.

[10] M. J. Katz, Fractals and the analysis of waveforms, Computers in biology and medicine 18 (3) (1988) 145–156.

[11] S. Hariri, M. C. Kind, R. J. Brunner, Extended isolation forest, IEEE transactions on knowledge and data engineering 33 (4) (2019) 1479–1489.

[12] R. B. de Santis, M. A. Costa, Extended isolation forests for fault detection in small hydroelectric plants, Sustainability 12 (16) (2020) 6421.